Spring 2016

Laser sintering and aerosol printing of conductive nanoparticles

Mahati Guntupalli

Department:

LASER SINTERING AND AEROSOL PRINTING OF CONDUCTIVE NANOPARTICLES

By

MAHATI GUNTUPALLI

A THESIS

Presented to the Faculty of the Graduate School of the

MISSOURI UNIVERSITY OF SCIENCE AND TECHNOLOGY

In Partial Fulfillment of the Requirements for the Degree

MASTER OF SCIENCE

In

MECHANICAL ENGINEERING

2016

Approved

Heng Pan, Advisor

Frank Liou

Edward C Kinzel

PUBLICATION THESIS OPTION

This thesis consists of the following article that has been submitted for publication. This article has been formatted according to Missouri S&T specifications.

Paper I, Pages 3 – 19 have been submitted to the APPLIED PHYSICS LETTERS.

ABSTRACT

Fabrication and printing of nanoparticles is an essential step in the manufacturing of low cost- high efficiency electronic devices. High material costs of noble metal particles necessitates the investigation for a potential substituent. Conventional methods of manufacturing are time consuming and uneconomical, thus intense research is being done to employ new methods for cost, time and space effective manufacturing process.

The first part of the thesis presents the fabrication of Copper nanoparticles. As an economical substituent for noble metal nanoparticles, Copper nanoparticles satisfy various properties as conductive inks, simultaneously suffering from the vital problem of oxidation. The acceleration effects of GO on photothermal laser–raster reduction of CuO nanoparticles are reported for the first time ever in this study. Transient emission studies revealed the dynamics of the reduction and the relationship between the emission signal and degree of reactions thereby providing novel approaches to detect and control thermal processing.

The second part of the thesis focuses on establishing and characterizing a direct write Aerosol jet printing system. A number of process parameters influence the deposition phenomenon, they are flow rate of carrier gas, stage speed, and distance of deposition head from substrate and nature of the substrate. In this study, the effect of these parameters on the deposition of ink is observed. The study provides an operability window and locates the regime for printing of thin silver lines in one pass.

ACKNOWLEDGEMENTS

I express my sincere gratitude to my advisor Dr. Heng Pan for the opportunity to be a member in Multi Scale Manufacturing Lab, for opportunity to work in his challenging research. He has been very supportive and always found time to guide me through any roadblock. I am also thankful for his financial support through my graduate studies and for his patience, motivation and enthusiasm.

I would like to thank the members of my thesis committee Dr. Frank Liou and Dr. Edward C. Kinzel for their insightful comments.

I thank Eric Bohanann, Jessica TerBush from the material characterization team for their help in my study.

I was blessed to be a part of a wonderful research group- Brendan Ludwig, Shou Wan, Joshua Staggs, Gopi Krishnan. I thank all of them for their help with my study.

I would not have made it this far without the continuous support and encouragement from my family, especially my parents and my sister.

TABLE OF CONTENTS

LIST OF ILLUSTRATIONS

LIST OF TABLES

1. INTRODUCTION

Fabrication and printing of nanoparticles in an essential step in the manufacturing of low cost- high efficiency electronic devices. High material costs of noble metal particles necessitates the investigation for a potential substituent. Conventional methods of manufacturing are time consuming and uneconomical, thus intense research is being done to employ new methods for cost, time and space effective manufacturing process. Noble metal nanoparticles have wide applications in the field of microelectronics. Their developing applications on the industrial level are hindered by low availability and high costs. Thus, as an alternative substituent, extensive research is conducted on Copper Nanoparticles to replace noble metal nanoparticles. Several methods in past have been proposed to for fabrication Copper Nanometal Particles. Addressing the oxidation issue and high manufacturing costs have been the prime objective towards this research. The thesis consists of two parts, Part I is an article on Photo thermal Laser raster reduction of Copper Oxide assisted by Graphene Oxide and Part II talks about Aerosol Jet Printing process and the variation in printing with change in parameters.

The first part of the thesis as discussed presents the fabrication of copper nanoparticles. As an economical substituent for noble metal nanoparticles, copper nanoparticles satisfy various properties as conductive inks, simultaneously suffering from the vital problem of oxidation. The acceleration effects of GO on photothermal laser–raster reduction of CuO nanoparticles are reported for the first time ever in this study. Transient emission studies revealed the dynamics of the

reduction and the relationship between the emission signal and degree of reactions thereby providing novel approaches to detect and control thermal processing. The study aims towards the development of a cost effective method in fabricating Copper Nanoparticles also addressing the oxidation issue during the fabrication.

The second part of the thesis focuses on establishing and characterizing a direct write Ultrasonic Aerosol jet printing system. Aerosol printing system is an unique continuous line printing system that can be used to print thin lines for microelectronic applications. A number of process parameters such as flow rate of carrier gas, stage speed, and distance of deposition head from substrate and nature of the substrate play an important role in the deposition phenomenon. In this study, the effect of these parameters on the deposition of ink is observed. This study provides a range of operation of the ultrasonic aerosol jet printing system. This operation range obtained is believed to help in printing continuous lines which can be used in manufacturing of several electronic devices. Further, a fundamental study was performed to understand the effect of nature of substrate on the deposition of individual droplets. This gave an opportunity to understand the interaction of ink with the substrate that is deposited on the surface through aerosol jet of the substrate.

PAPER

I. PHOTOTHERMAL LASER-RASTER REDUCTION OF COPPER OXIDE BY GRAPHENE OXIDE

ABSTRACT

Copper nanoparticles, as an economical substituent for noble metal nanoparticles satisfy various properties as conductive inks, concurrently suffering from the vital problem of oxidation. Existing fabrication methods use inert gas protection or complex chemical processes to avoid oxidation that increases cost offsetting the benefits of copper. In this study, the acceleration effects of GO on photothermal laser–raster reduction of CuO nanoparticles are reported for the first time ever. Further transient emission studies revealed the dynamics of the reduction and the relationship between the emission signal and degree of reactions thereby providing novel approaches to detect and control thermal processing.

Key words: Laser-raster reduction, Photothermal, Graphene oxide, Copper nanoparticles

1. INTRODUCTION

Conductive nanoparticles have attracted much attention due to their potential application in fabrication of low cost and sophisticated devices like sensors, radio frequency identification antennas and interface modules for mobile phones on flexible substrates [1]-[3]. Conductive polymers, carbon, graphene and metallic inks have been used in the formation of conductive tracks. Among all the materials, silver nanoparticles are the most commonly used with rapidly developing applications. However, its low availability and high costs limit its wide industrial application. It is only natural to look for an economic substitute for the silver nanoparticles. Copper nanoparticles being relatively cheaper are considered to be an alternative to silver particles due to its conductive properties [4]-[5] optical [6] and catalytic properties [7]. With the decrease in size of the nanoparticles there is a drastic increase in the oxidation of CuNPs while fabrication because of increasing surface area [8].

A few successful attempts were made to solve this problem. Among them, are the electrodeposition of core shell copper-silver nanoparticles [9], thermal evaporation under high ultra-vacuum ion exchange in soda lime glass or transmetalation process [10]. However, none of these effectively reduce the cost of manufacturing of CuNPs. Other ways of fabricating CuNPs were through [9] sonochemical reduction method [11], microemulsion techniques [12], [13], polyol processes [14], metal vapor synthesis [15], vacuum vapor deposition [16] and super-critical methods [17], [18]. Most of the processes are either carried out in inert atmosphere or involves complex chemical processes.

Graphene oxide has been found to be effective in assisting many reactions like carbonization and reduction reactions [19]-[21]. Graphene oxide reduced by laser and other chemical methods has wide applications in electronic devices [22]-[25]. This study reports the catalytic behavior of graphene oxide in assisting the reduction of copper oxide particles by photothermal laser raster reduction. It illustrates and proves the emission – temperature reaction relationship. A novel emission based control of the process is proposed as findings in this study.

2. EXPERIMENTAL SET-UP

A solid state, Q-switch TEMoo- Mode Nd-YAG laser (Lee Lasers, 1064nm) was used with an average power 40 Watts, CW/pulsed. The laser spot size is approximately 300 μm in diameter. A camera is placed focusing on the area being processed on the XYZ translation stage, to monitor the process. Two photo diodes detectors PD1 and PD2 (Thorlabs) were placed to collect the transient emission signals during the laser processing. An oscilloscope with a nanosecond resolution was used to record the transient signals of the process. A visible NIR spectrometer (Ocean Optics) was placed to collect the emission spectrum during the laser processing. A galvanometer was aligned with laser beam to measure the power of the laser corresponding to each experiment performed. The set up described above is depicted in the figure 2.1 below.

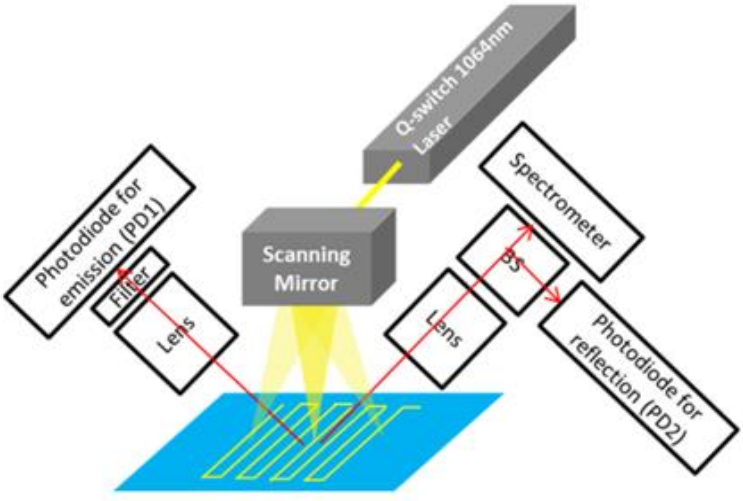

Figure 2.1. Image showing the laser experimental set up

2.1. FABRICATION OF FILMS OF COPPER OXIDE AND GRAPHENE OXIDE

Copper Oxide (CuO) particles of ~5 μm in diameter were dispersed with Graphene Oxide (GO) flakes in ethanol. GO flakes used in this study were synthesized by using modified Hummer method 26-27. The dispersion was heated to 120ºC and dried to obtain the homogenous free standing films. The films were peeled after they dried. The ratio of the mixture of CuO particles and GO flakes was varied by weight to obtain the different concentration films for experimentation. The figure 2.2 describes the schematic diagram for fabricating the samples during experiment.

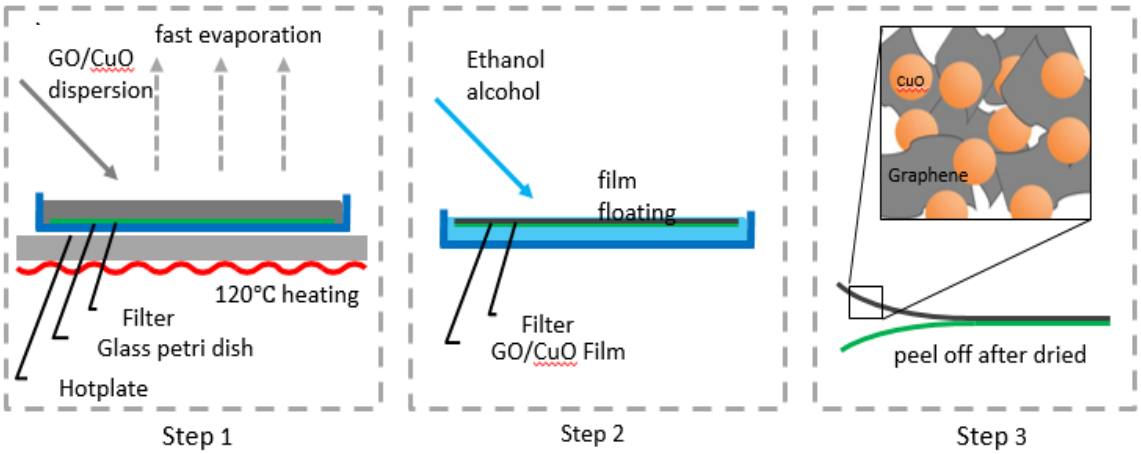

Figure 2.2. Images describing the process of film fabrication for sample preparation

3. RESULTS AND DISCUSSIONS

Understanding the laser process parameters is very important as they control the amount of energy being input to the sample for sintering. The process parameters play an important role in determining the degree of reduction. Since the samples are several microns in thickness, laser power of 1% corresponding to 5 W was chosen. A frequency of 1 KHz, pulse width of 1000 µs were used with step period of 250 µs to study the reduction process. 1:1 CuO and GO films and GO samples we were processed with above parameters. The figure 3.1 indicates the relation of step size to dwell time and pattern used to ensure complete processing of the sample.

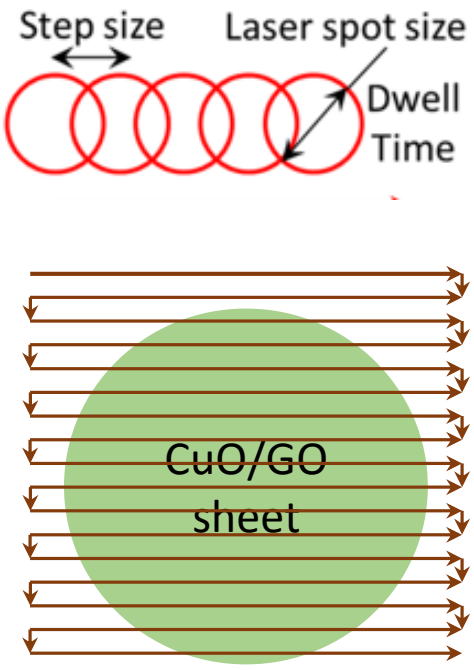

Figure 3.1. Laser processing parameters and pattern

The earlier combination was used to process 5%, 10%, 25% and 50% GO/CuO samples to understand the effect of GO on reduction efficiency. The efficiency of reduction of GO on GO/CuO composites was studied for all the samples using X-Ray Diffraction (XRD). The peaks of copper and its oxides are identified and indicated in figure 3.2.

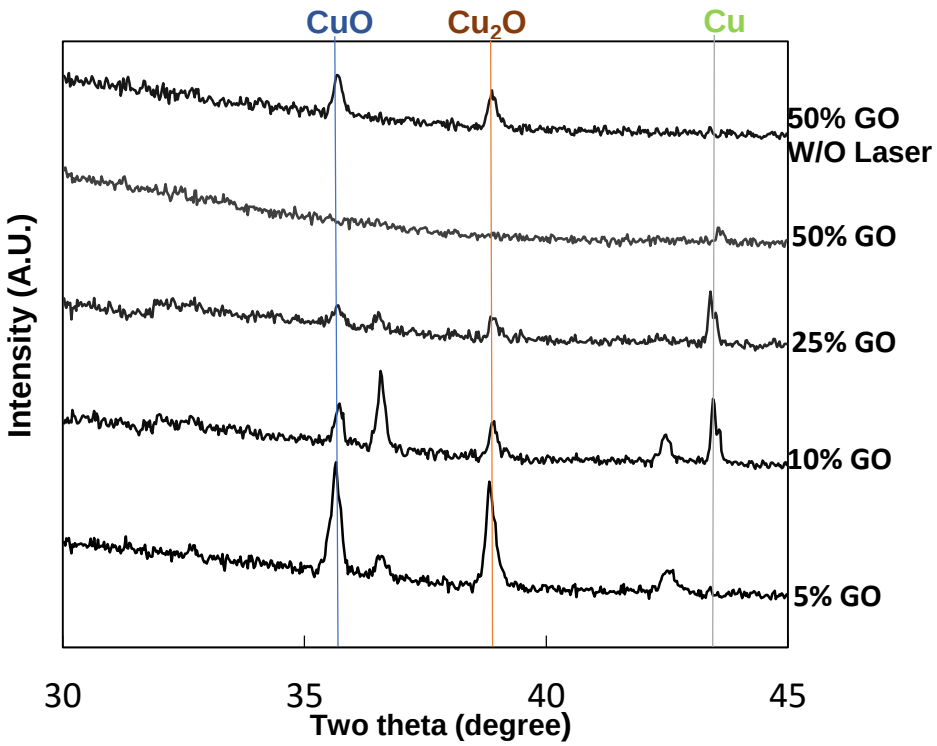

Figure 3.2. XRD Spectrum of samples with different GO concentrations

A clear trend was noticed in peaks of oxides of copper with change in the percentage of GO in the samples. The oxide peaks reduce with the increase in the

amount of GO in the sample. Also, when compared to the as prepared sample of 50% GO/CuO, the processed sample has no other noticeable peak other than a copper peak. Alternatively, the reduction becomes more pronounced as GO fraction increases. As all the samples were subjected to the same conditions of laser processing, the above result is a direct evidence of GO acceleration on CuO reduction.

To further prove the acceleration effect, optical reflectance studies were performed on the samples with different GO concentration with varying dwell time. With the increase in GO concentration and the increasing dwell time the reflectance of the films shifts towards near infrared region exhibiting clear characteristic Cu reflectance spectrum as shown in figure 3.3.

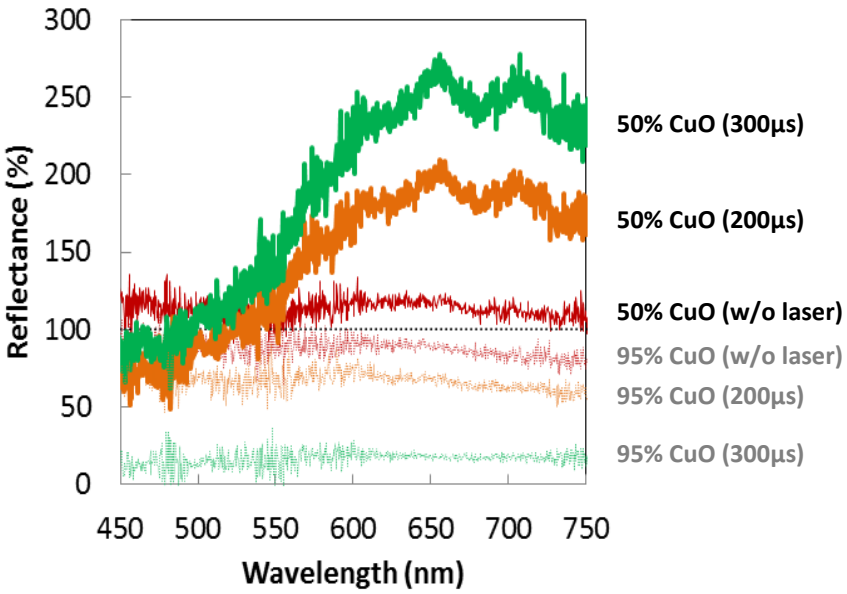

Figure 3.3. Reflectance comparison of films with different GO fraction subjected to different dwell time

The plotted reflectance is the ratio between the measured reflectance to the reflectance measured by a 3 μm thick GO sample. The films with lower GO fractions (5%) show a decay in the reflectance spectrum. Reflectance fading observed here could be the result of laser processing induced particle agglomeration and scattering. The plotted reflectance is the ratio between the measured reflectance to the reflectance measured by a 3 μm thick GO sample. The films with lower GO fractions (5%) show a decay in the reflectance spectrum. Reflectance fading observed here could be the result of laser processing induced particle agglomeration and scattering.

To understand the reaction dynamics transient emission studies were performed on samples with different thickness and composition shown figure 3.4 (a) inset. Figure 3.4 (a) and (b) shows that emission growth is always accompanied by a reflection reduction. Reflection measurements revealed that the reflection signal fading was a result of GO reduction to RGO, subsequent laser heating on RGO enhanced the emission signal. Thicker GO films absorb more energy and hence the higher emission observed proved the earlier statement. Hence, emission intensity can be an indirect representation of accumulated energy in the film. Figure 3.4 (c) and (d) show that CuO addition greatly suppressed the emission signal, indicating reduction in accumulated energy. It can thus be inferred that the extra energy was dissipated to heat, reduce, and melt or even evaporate CuO. Investigations were then made to co-relate film temperature with the emission signals, to understand the degree of reduction, and understanding the reaction dynamics.

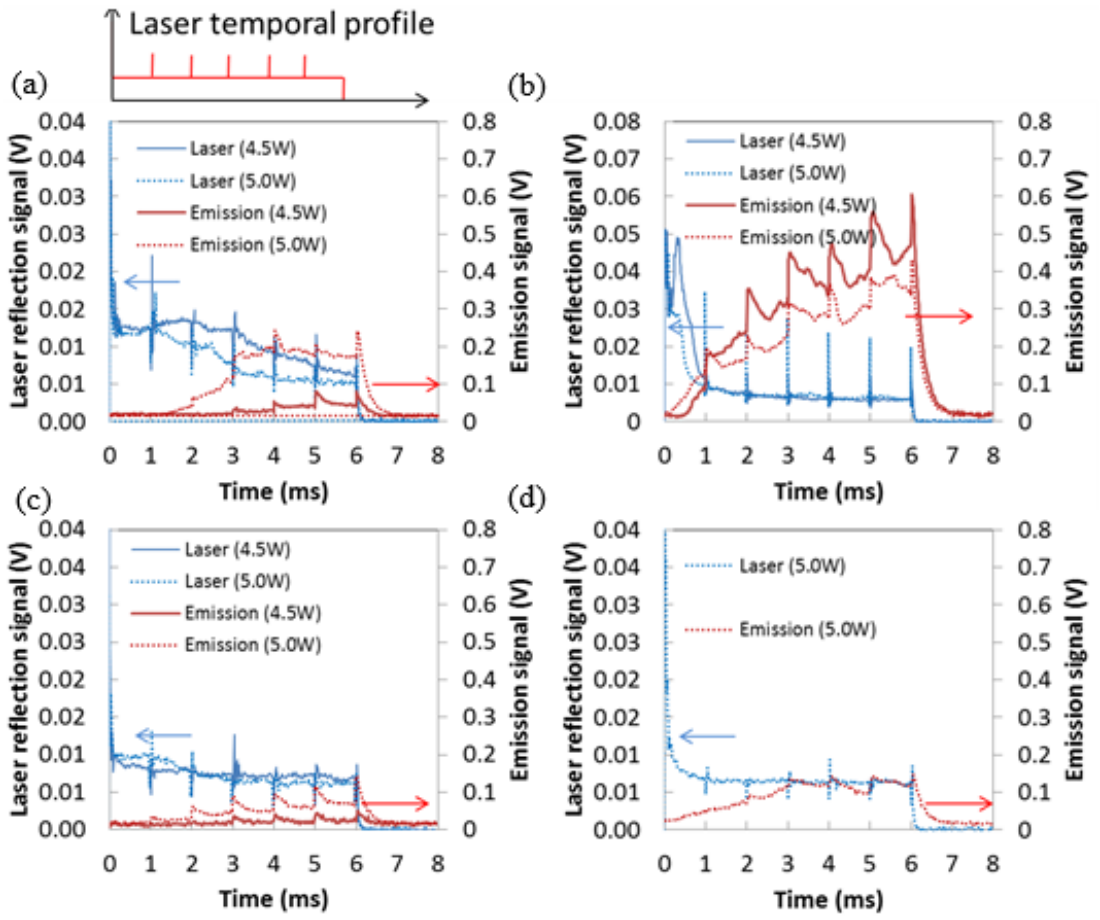

Figure 3.4. Transient emission studies on (a) 3 µm GO, (b) 6 µm GO, (c) 7 µm GO/CuO, and (d) 12 µm GO/CuO films with a laser pulse of 6ms. The inset figure above (a) is the laser temporal profile used in the tests

Emission spectrum of the samples was collected while processing with different laser powers. On comparing the representative emission spectrums (figure 3.5), we could notice a peak located at ~630 nm. Clearly from the figure, emission occurred at higher energies than the energy of the exciting photons (1064 nm) suggesting the participation of multiphoton processes in this emission [29]. It was previously reported that the up-conversion and broadband emission is related to thermal effects [30], which provides strong support to this study to correlate

emission signal with film temperature and reduction degree. The emission signal at 630 nm as we can see in figure 3.5 is non- linear with increasing laser power.

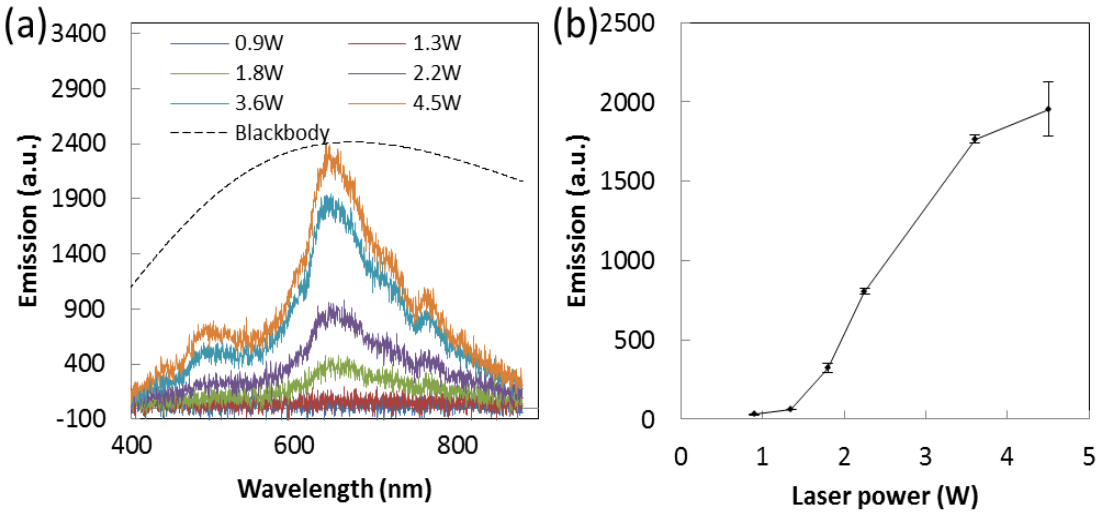

Figure 3.5. Emission signals collected at different laser powers (a) *In-situ* collected representative emission spectrums under various laser powers, and (b) emission signals collected at 630 nm under different laser powers

The above discussion suggests the non-linearity in the thermal effects produced in the emission and optical absorption. The theory of blackbody radiation is naturally the first choice to interpret the emission spectrum obtained from the experiment. A significant mismatch can be noted on comparing the emission spectrum with the representative spectrum of the blackbody at T=4315K. Also, a blue shift of the emission band at peak wavelength should be observed with increasing temperature (power). There was no such spectral shift noticed and all

the peaks seem to occur at 630 nm to as found in figure 3.5 a. The temperature reached in the sample is expected to be considerably lower when compared to the representative blackbody temperature to produce a white light spectrum at 630 nm.

In order to validate the relevance between emission and possible film temperature, the emission signal and XRD pattern was collected for a large area raster-scanning with various dwell times. Study of these samples show a strong dependence on the emission intensity to dwell time. Figure 3.6 (a) reveals a non-linear relation in the emission signal and the dwell period.

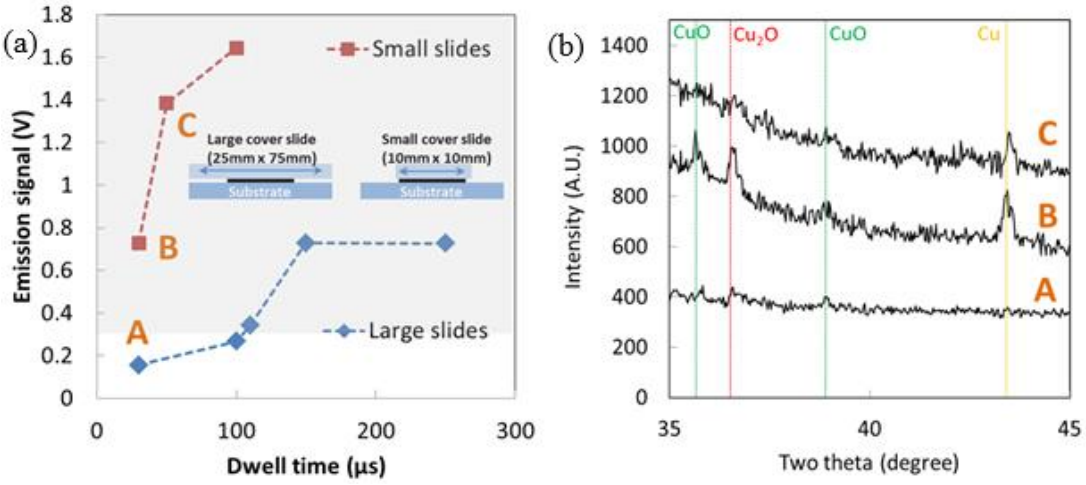

Figure 3.6. Emission and XRD signals of processed samples at various dwell time. (a) Emission signal collected with different step periods (b) XRD Pattern of composite film processed

Comparing XRD patterns of sample A and B that are only different in cover size (influencing the local temperature). we found that clear Cu peaks only appeared in sample B. Emission signal intensity was also found be controlled by controlling the size of the cover slide on the samples, which effects local film temperature revealing a clear relation among emission intensity, film temperature and reduction degree. This relation is very evident and can be revealed from figures 3.6(a), 3.6(b).

This result indicated that higher local temperature (smaller slides) enhanced reduction and emission signals. Comparing XRD patterns obtained from sample B and C that are only different in dwell time, it was found that CuO peaks disappeared in sample C. This result indicated that longer dwell time resulted better reduction, which is consistent with previous experiment results. As it can be concluded, higher local temperature results in higher emission intensity, therefore more pronounced reduction. Therefore, the emission signal could provide indication of the film temperature and the degree of reduction.

Figure 3.7 (a), (b) in the following page compares the emission signal and XRD patterns of samples processed by different laser powers. The emission signal increased and the Cu peak in XRD pattern became more and more pronounced with increasing laser power, which indicated higher degree of reduction. The non –linear co-relation can be seen in the variation of power over the emission signal intensity and thus it pronounces our previous statement of the increase in the emission with increasing laser power and degree of reduction.

SEM analysis of these cover glass samples obtained from process as in figure 3.6, revealed Cu nanoparticles of ~ 50 nm in diameter. In all the samples, with emission signals 0.3 V and above, deposited/transferred particles and transferred particles were noticed on the cover glass. Since only micron sized particles of CuO were used to conduct this study, the appearance of nano-sized particles on the cover glass is an indication that there was evaporation (at about 2000°C) and re-deposition of particles on the cover glass.

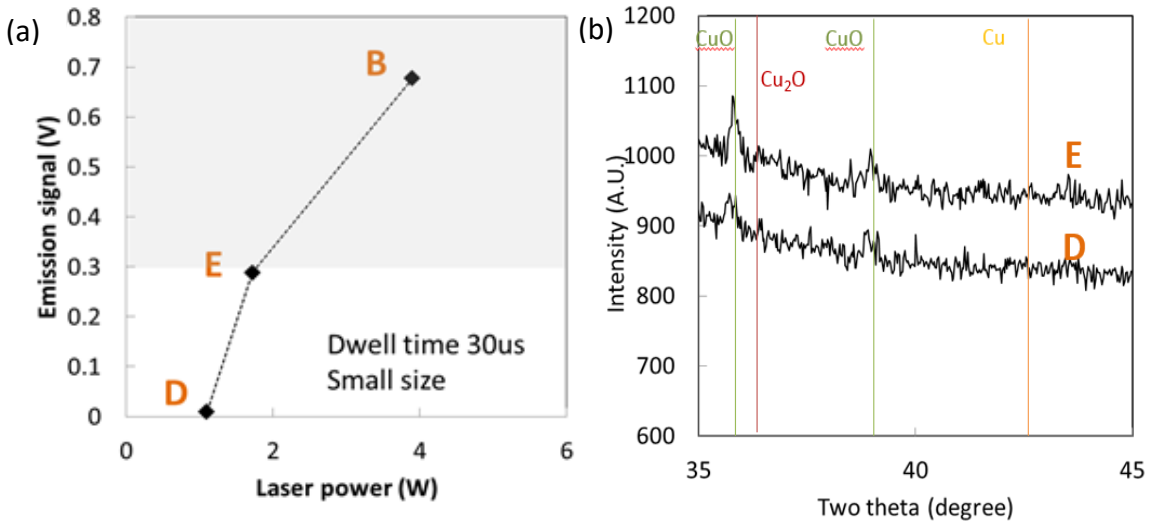

Figure 3.7. Emission and XRD signals of processed samples at various laser power (a) Emission signal collected with different laser power (b) XRD Pattern of the samples corresponding to the letters in the emission to plot

Thus, through this study we not only validated the relevance between the emission signal and the local film temperature, but also provided a quantitative estimations of relating emission signals to temperatures. Our promising potential

application of this relationship is to infer the processing result from in-situ white light emission. White light emissions in observed in this laser study are much stronger and detectable when compared to conventional thermal black-body radiation temperature measurement. Further investigations on the nature of white light emission will be valuable for online process of thermal processing on GO or graphene composite films.

4. CONCLUSIONS

A photothermal laser raster reduction of the composite film was carried out and acceleration effect of GO on CuO reduction was proved my XRD and optical reflectance studies. The dynamics of the reaction was studied while processing and the relationship between emission intensity, temperature and the degree of reduction was revealed. The study has resulted in a low cost energy efficient solution to the oxidization issue of copper by catalysis property of GO. The in situ reaction study provides a novel approach towards control of thermal processing using emission signals.

5. BIBLIOGRAPHY

[1] S. Koskinen, L. Pykäri, and M. Mäntysalo, “Electrical performance characterization of an inkjet-printed flexible circuit in a mobile application, ”*IEEE Trans. Compon., Packag., Manuf. Technol.*, vol. 3, no. 9, pp. 1604–1610, Sep. 2013.

[2] B. S. Cook, J. R. Cooper, and M. M. Tentzeris, “An inkjetprinted microfluidic RFID-enabled platform for wireless lab-on-chip applications,” *IEEE Trans. Microw. Theory Techn.*, vol. 61, no. 12,pp. 4714–4723, Dec. 2013.

[3] V. Pekkanen *et al.*, “Utilizing inkjet printing to fabricate electrical interconnections in a system-in-package,” *Microelectron. Eng.*, vol. 87, no. 11, pp. 2382–2390, 2010.

[4] Kim H S, Dhage S R, Shim D E and Hahn H T; Intense pulsed light sintering of copper nanoink for printed electronics 2009 Applied Physics A 97 791.

[5] Lee Y, Choi J R, Lee K R, Stott N E and Kim D Large-scale synthesis of copper nanoparticles by chemically controlled reduction for applications of inkjet-printed electronics; 2008 Nanotechnology 19 415604.

[6] Thi My Dung Dang, Thi Tuyet Thu Le, Eric Fribourg-Blanc and Mau Chien Dang; Synthesis and optical properties of copper nanoparticles prepared by a chemical reduction method, Nanotechnology 19 (2008) 415604.

[7] Grouchko, M.; Kamyshny, A.; Ben-Ami, K.; Magdassi, S. Synthesis of copper nanoparticles catalyzed by pre-formed silver nanoparticles. J. Nanopart. Res. 2009, 11, 713-716.

[8] Jeong, S.; Woo, K.; Kim, D.; Lim, S.; Kim, J. S.; Shin, H.; Xia, Y.;Moon, J. Architectural Growth of Cu Nanoparticles Through Electrodeposition Adv. Funct. Mater. 2008, 18, 679–686.

[9] Ng, K.H.; Penner, R.M. Electrodeposition of silver-copper bimetallic particles having two archetypes by facilitated nucleation. *J. Electroanal. Chem.* 2002, *522*, 86-94.

[10] Dhas NA, Raj CP, Gedanken A (1998) Synthesis, characterization and properties of metallic copper nanoparticles. Chem Mater 10:1446–1452.

[11] Kumar, R.V.; Mastai, Y.; Diamant, Y.; Gedanken, A. Sonochemical synthesis of amorphous Cu and nanocrystalline Cu2O embedded in a polyaniline matrix. J. Mater. Chem. 2001, 11, 1209-1213.

[12] Lisiecki, I.; Pileni, M.P. Synthesis of copper metallic clusters using reverse micelles as microreactors. JACS 1993, 115, 3887-3896.

[13] Qi, L.M.; Ma, J.M.; Shen, J.L. Synthesis of copper nanoparticles in nonionic water-in-oil micro-emulsions. J. Colloid Interface Sci. 1997, 186, 498-500.

[14] Park, B.K.; Jeong, S.; Kim, D.; Moon, J.; Lim, S.; Kim, J.S. Synthesis and size control of monodisperse copper nanoparticles by polyol method. J. Colloid Interface Sci. 2007, 311, 417-424.

[15] Vitulli, G.; Bernini, M.; Bertozzi, S.; Pitzalis, E.; Salvadori, P.; Coluccia, S.; Martra, G. Nanoscale copper particles derived from solvated Cu atoms in the activation of molecular oxygen. Chem. Mater. 2002, 14, 1183-1186.

[16] Liu, Z.W.; Bando, Y. A novel method for preparing copper nanorods and nanowires. Adv. Mater. 2003, 15, 303-305.

[17] Kirk J Ziegler, R Christopher Doty, Keith P Johnston, and Brian A Korgel, J Am Chem Soc 123 (32), 7797 (2001).

[18] Joanna P Cason and Christopher B Roberts, The Journal of Physical Chemistry B 104 (6), 1217 (2000).

[19] Yuanyuan Li, Hongli Zhu, Fei Shen, Jiayu Wan, Xiaogang Han, Jiaqi Dai, Hongqi Dai, and Liangbing Hu, Advanced Functional Materials 24 (46), 7366 (2014).

[20] Deepti Krishnan, Kalyan Raidongia, Jiaojing Shao, and Jiaxing Huang, ACS nano 8 (1), 449 (2013).

[21] Yanwu Zhu, Shanthi Murali, Weiwei Cai, Xuesong Li, Ji Won Suk, Jeffrey R Potts, and Rodney S Ruoff, Adv Mater 22 (35), 3906 (2010).

[22] TN Narayanan, Zheng Liu, PR Lakshmy, Wei Gao, Yutaka Nagaoka, D Sakthi Kumar, Jun Lou, Robert Vajtai, and PM Ajayan, Carbon 50 (3), 1338 (2012).

[23] Pei Dong, Yu Zhu, Jing Zhang, Cheng Peng, Zheng Yan, Lei Li, Zhiwei Peng, Gedeng Ruan, Wanyao Xiao, and Hong Lin, The Journal of Physical Chemistry C 118 (45), 25863 (2014).

[24] Jiayan Luo, Vincent C Tung, Andrew R Koltonow, Hee Dong Jang, and Jiaxing Huang, J Mater Chem 22 (26), 12993 (2012).

[25] Seung Hwan Ko, Jaewon Chung, Heng Pan, Costas P Grigoropoulos, and Dimos Poulikakos, Sensors and Actuators A: Physical 134 (1), 161 (2007).

[26] Daniela C Marcano, Dmitry V Kosynkin, Jacob M Berlin, Alexander Sinitskii, Zhengzong Sun, Alexander Slesarev, Lawrence B Alemany, Wei Lu, and James M Tour, ACS nano 4 (8), 4806 (2010).

[27] Jiayu Wan, Feng Gu, Wenzhong Bao, Jiaqi Dai, Fei Shen, Wei Luo, Xiaogang Han, Danial Urban, and Liangbing Hu, Nano letters (2015).

[28] Strek, W.; Cichy, B.; Radosinski, L.; Gluchowski, P.; Marciniak, L.; Lukaszewicz, M.; Hreniak, D., Laser-induced white-light emission from graphene ceramics–opening a band gap in graphene. *Light: Science & Applications* 2015**,** *4* (1), e237.

[29] Wang, J.; Tanner, P. A., Upconversion for white light generation by a single compound. *J Am Chem Soc* 2009, *132* (3), 947-949.

SECTION

2. AEROSOL JET PRINTING

2.1 INTRODUCTION

Solution processes involving various kinds of nanomaterials are widely studied in the field of printed and flexible electronics in search of new manufacturing processes with increase in productivity and reduction in energy consumption over conventional processes. Aerosol jet printing is a non-contact, mask-less printing that enables high resolution printing with fine pitch. It is an additive manufacturing technology used to controllably deposit features onto samples in patterns defined by computer-aided design/ computer aided manufacturing (CAD/CAM) software allowing rapid prototyping of various geometries without the use of lithography [1, 2]. Aerosolized droplets from the nebulizer (pneumatic or ultrasonic) are concentrated and directed towards the substrate through the carrier flow gas. An annular flow of sheath gas is added to the carrier gas flow at the deposition head in the commercial Aerosol Jet Printer patented by Optomec. The gases occupy the outer layer of the flow, the layer adjacent to the walls of the tube and needle, acting as a focus mechanism, limiting the aerosol to be in the center of the flow. This reduces the excess of dispersion of the aerosol particles producing focused clean lines. The commercial aerosol system, Optomec is capable of printing lines of 10 µm to 5 mm in width. The advantage of aerosol printing is its large standoff distance (1 mm- 5 mm) thus simplifying printing over irregular substrate. Process not being sensitive to

environment can be carried at room temperature, providing an opportunity for wide variety of substrates to print. King and Renn [8] described the advantages of aerosol printing- being maskless approach reduces the time for product development, lower costs associated with mask set up for initial small production runs and greater material utilization reducing the cost of manufacturing and is thus more environmentally friendly.

Maiwald et al. [9] reported the creation of strain gauges for non-destructive testing using Aerosol Jet Printing. Folgar et al. [10] produced multilayer structures using ceramic based inks printed with aerosol jet to form capacitors. Silver conductive lines were printed on plastic and printed circuit boards (PCBs) for using in a chemisensor, to detect the nerve gas [11]. A lot complicated multi-layer devices were built by Ha et al. [12] and Cho et al. [13] using Aerosol jet for TFTs with a printed CNT active layer. Thin wafers (100 μm) can be used without any breakage unlike the contact print methods, giving higher number of solar cells per Si single crystal boule [14, 15].

Many applications of the aerosol based direct write for microelectronics were summarized by Justin et al. [16]. However, not many reports are made studying the factors effecting the quality of printing. Goth et al [17] studied the silver printed lines using various flow rates and stage speeds through an aerosol jet printer that used a pneumatic atomizer. However, the thickness was controlled through the number of layers deposited. Verheecke et al. [18] also studied characteristics of printing with a pneumatic atomizer representing the effect of three gas flow rates on the edge definition of the printed lines. The above

mentioned studies give a broad understanding of factors influencing the line characteristics but they are limited to the pneumatic atomizer. For an ultrasonic atomizer, Mahajan et al [19] has reported a study of line geometry with varying stage speed, carrier gas flow rate and focusing ratio using a commercial Aerosol Jet Printer (M^3D, Optomec Inc.). The article discusses the importance of focusing ratio (ratio of sheath gas flow rate to carrier gas flow rate) in the printing process and the line width obtained under optimum conditions was 20 µm with an aspect ratio 0.1.

An aerosol experimental set up with an ultrasonic particle generator is established comparable to the set up in article by I.S. Akhatov et al. [20]. A deposition head was fabricated and assembled to the particle generator. Printing capabilities of this machine are recognized and the geometrical features are characterized. The study of influencing parameters like stage speed, carrier gas flow rate, deposition head and substrate effects were studied giving a good knowledge of the functioning of the established system. The results obtained provide detailed understanding on the operational range of the system and the process regime to obtain the best prints.

2.2 EXPERIMENTAL SET UP AND METHODS

An ultrasonic particle generator (Sonozap 2.4 MHz 241 PG) is used for atomization to generate droplets of various sizes. Droplets of a few microns or sub-microns in size are carried with the exhaust and the larger particles with high inertia condense in the vial. The rate of particle generation could be changed from 0-

100% of the full output capability. The carrier gas flow rate (N_2, 99%) into the aerosol system is controlled by MKS Model M100B01322CP1BV mass flow controllers (upto 200 SCCM flow, 1% full scale accuracy). The substrate is maintained at the room temperature on a motorized translation stage (Newport-UTM50CC.1). The figure 2.1 describes the principle diagram indicating the atomizer in the particle generator vessel and the deposition head over a linear control table.

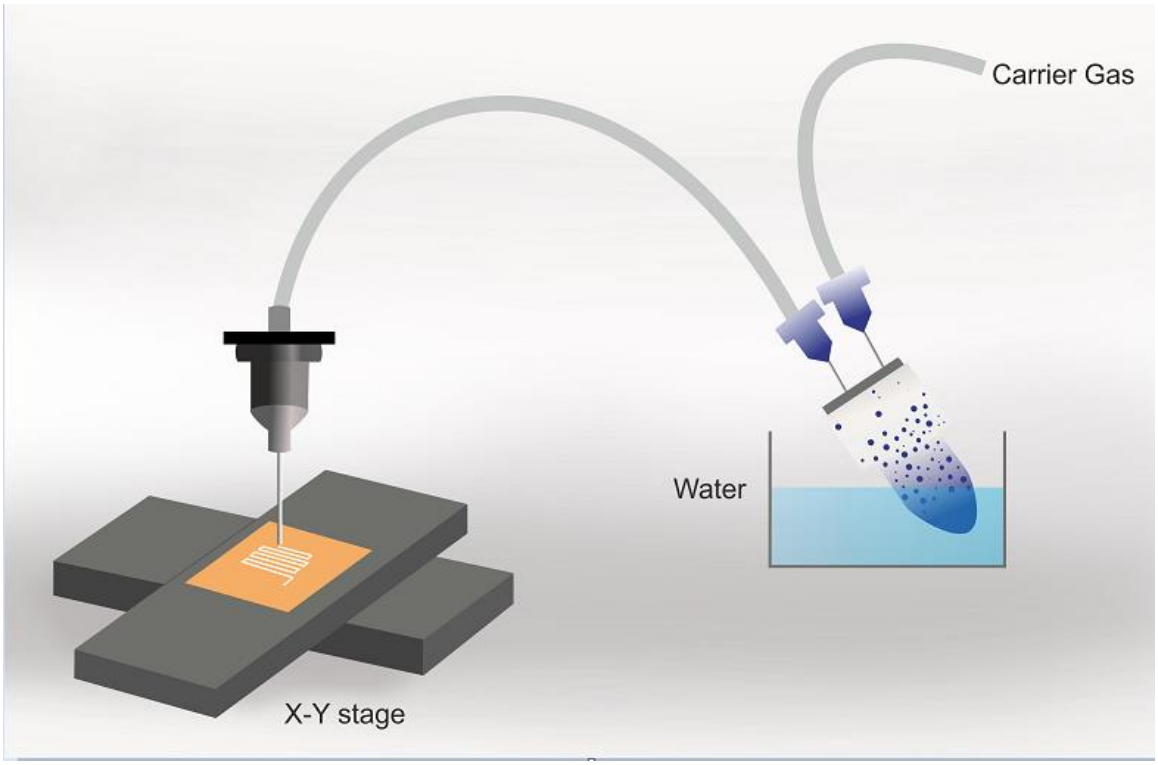

Figure 2.1. Aerosol Jet Printing set up

A 1.5 ml Teflon coated micro-centrifuge vial, (Savillex) is used for generating the micro-particles. The vial is air sealed with two openings, an inlet for the carrier gas and an outlet for micro-particles to the deposition head. Figure 2.1 shows the position of the ideal position of the vial. It is positioned with an inclination to the wall to gain more surface area exposed to the resulting in better atomization. Since the vial is Teflon coated the nebulized droplets do not stick to the walls unlike the contemporary glass vial. Commercial Ag ink (UTDOTS), 30-40wt% silver was used for printing throughout the experiment.

The deposition head in this experimental set up consists of a 3D printed part press-fit to a standard cage plate (Thor Labs) then mounted on a translational/ rotational stage. The tube consisting of the aerosol exhaust was directly connected to the deposition needle held by the 3D printed part. Two different kinds of deposition needles have been used, a Micro-nozzle (Subrex) and a metal needle (Musashi). The line geometry obtained from both the needles is compared in this study.

2.2.1 Effect of Process Parameters. A number of parameters influence the functioning of aerosol jet printing. Power of atomizer, carrier gas flow rate through the system, sheath gas flow rate, position of the vial in the actuator, working distance, temperature of the transmission liquid, substrate and stage speed (deposition speed). Many of the above parameters directly affect the atomization taking place in the particle generator. Additional factors influencing the printing are the surface tension, solids loading, temperature at which substrate is maintained and viscosity of the ink used. A detailed study of the other parameters

was made to develop the best operating conditions for effective printing in single pass.

Silver lines were printed with a constant level of water in the atomizer. An average of 20°C was maintained throughout the process. Flow rate in this discussion refers to the ‘carrier gas flow rate through the system’. Line properties are also influenced by height of deposition head. Stage speed and flow rate were varied from 0-2.5 mm/s and 0-55 sccm. Different kinds of nozzles/ needles were used to study the print. Needles of diameter 250 µs, 200 µs (Musashi) and micro-nozzles of diameter 150 µs and 100 µs (Subrex) were used to compare the line width and the flow rate. Nature of two substrates glass and Titanium coated surface were compared with respect to the particle deposition. Geometric characteristics of the lines were studied. Line thickness, line width was evaluated with varying flow rate and stage speed. The line width was measured for each sample and efforts were made to exclude the overspray in the measurement. The thickness of the line was measured using the Hirox 3D optical microscope.

2.3 RESULTS AND DISCUSSIONS

The quality of printing and features of the printed patterns, as discovered above, are determined by several process parameters and ink properties. In this study we will explore the key adjustable printing parameters such as carrier gas flow rate and stage speed, distance form nozzle to substrate and influence of substrate. For efficient study, all the other conditions were maintained constant and ink from same vendor was used throughout the experiment. The distance

between the nozzle tip and the surface of the substrate will be referred to as working distance. For each individual study the working distance was maintained constant. Each data point in the graph represents the average of data collected from a number of samples over completely randomized experiment and corresponding error bars were plotted calculating the standard deviation of the values. It is very natural to expect over spray along the printed lines. Image J software was used to measure the line width. Figure 2.2 shows the Hirox image, representing the evaluation of line thickness. The measurements correspond to 110 µm needle diameter. The profile of the line can be obtained as pointed in the line.

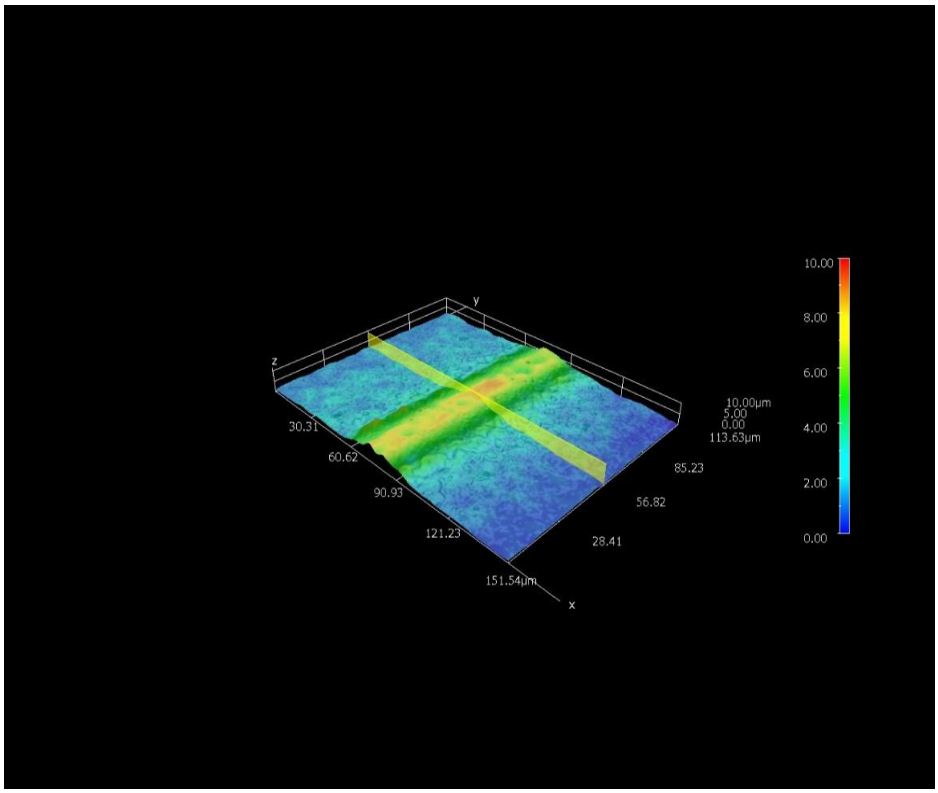

Figure 2.2. Image representing thickness evaluation using Hirox Microscope

A 2D profile is picked from the image to obtain the height of the printed line. Such samples were taken from different locations for number of samples to obtain average value of height for each combination. Figure 2.3 (a, b) show the variation of the line width and the line thickness with the change in the nozzle diameter for a constant flow rate (35 sccm), stage speed (1 mm/s) and from a working distance of 1 mm. As expected, smaller nozzles produce finer lines. However, in the smaller nozzle high flow rate lead to high pressure resulting in imperfect printing and clogging. This explains the wider error bar in the figure 2.3a.

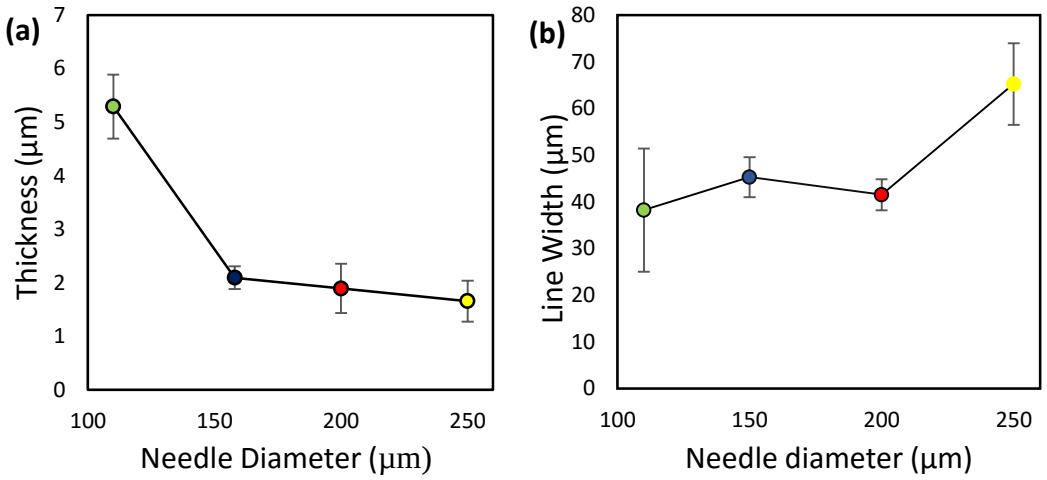

Figure 2.3. Line width and line thickness for different needle diameters (a) Plotting line width for different needle diameters (b) Plotting thickness of the lines printed with different needles

A clear difference can be noticed in the printing of lines at with different nozzle diameters as shown in figure 2.4. From the images and graphs discussed

earlier we can conclude that except for extremely wide lines, the desirable printing width can be achieved with diameter 150 µm and 200 µm needles. Lower flow rates would give better lines if needles with smaller diameter were to be used for deposition. This study involves the working of a micro- needle (200 µm, Musashi).

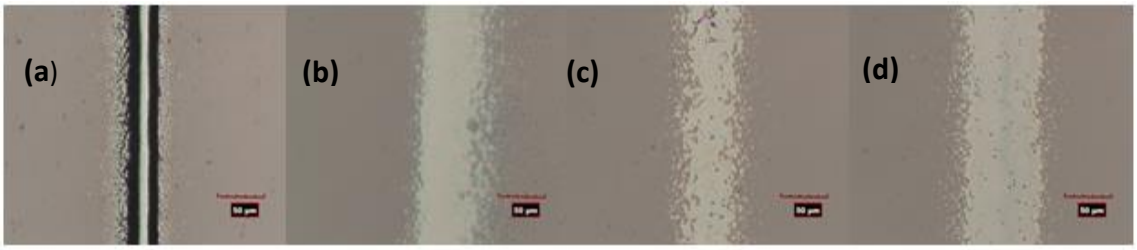

Figure 2.4. Images of lines printed with different diameter (a), (b), (c), (d) represent the images of the lines printed using needles 110, 150, 200, 250 µm

Figure 2.5 (a), (b) represent the varying line thickness with change in stage speed and gas flow rate respectively of lines printed using micro needle. The behavior of the system with respect to the stage speed and flow rate is as expected. The increase in gas flow rate results in increased line thickness. Deposition is irregular due to the high pressure developed in the needle at deposition head, resulting in larger error bars. Since, the rate of atomization and the stage speed (1 mm/sec) is maintained same throughout the experiment, there is a very clear indication of the change in thickness with flow rate resulting in high error. The explanation implies to lower rates as well. As the stage speed increases

and all the other factors remain constant, with flow rate (35 sccm) the thickness of the line decreases with increase in stage speed.

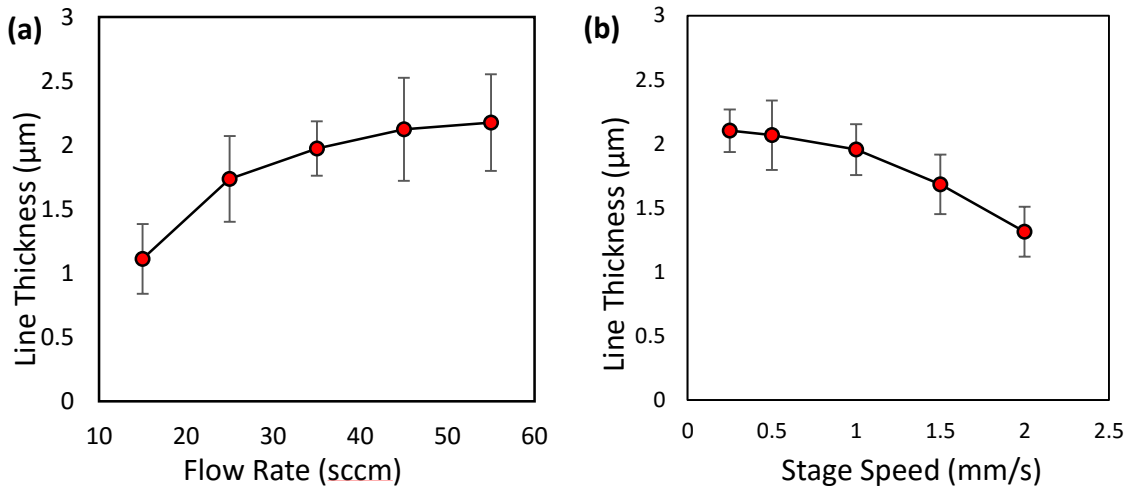

Figure 2.5. Images showing the variation in line thickness with varying parameters (a) Plot of line thickness with varying flow rate (b) Plot of line thickness with stage speeds

The line width varies over a wide range with the change in stage speed. As the amount of ink deposited at a particular instance of time decreases with the increase in stage speed. On the other hand, wide variation is not noticed in the line width the change in flow rate.

The figure 2.6 (a) describes the line width variation with the changing stage speeds for a constant carrier gas flow rate (35 sccm).

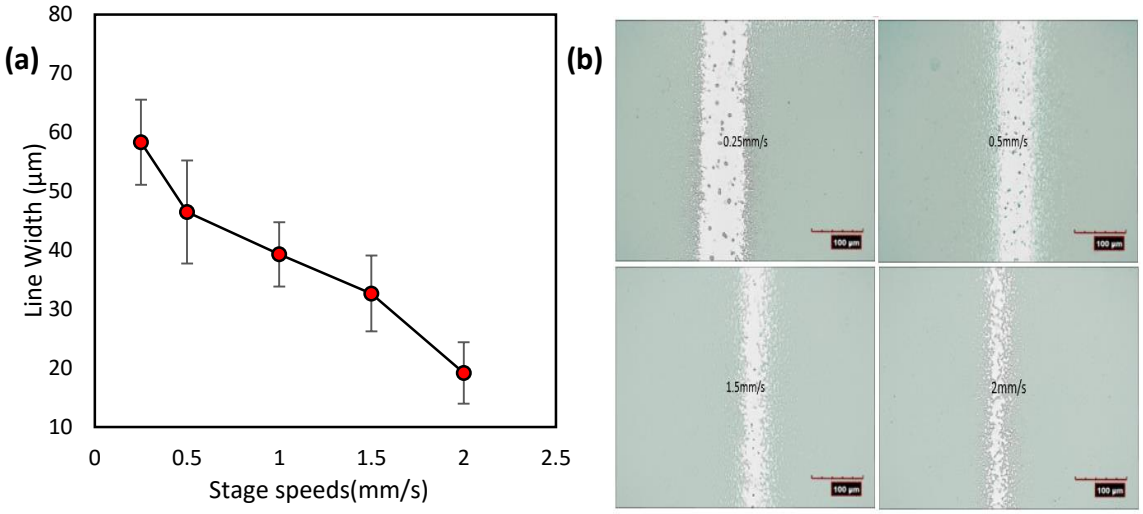

Figure 2.6. Images representing the variation in line width with varying stage speed (a) Plot line width with stage speeds (b) Figure showing the variation in line width with varying stage speeds

Figure 2.7 represents a set of images with increasing flow rate at a constant stage speed of 1 mm/s. The images below clearly represent, that there is no obvious trend in the line width with increase in the flow rate. It can be explained that the carrier gas from the deposition head flows along the interior walls of the needle and adjusts to the needle diameter, thus giving the same beam width. Hence, it can be concluded with the above explanation that the line width almost remains constant with changing flowrate and is highly dependent on the needle diameter.

Spreading of the ink on the surface of the substrate becomes an important factor in determining the line width. Certainly, at lower stage speed the accumulation of the ink at a deposition point would be more when compared to higher stage speed, hence explains the reason for the decrease in the line width

with increasing stage speeds. This phenomenon also explains for the increase in thickness of the line with increasing flow rate.

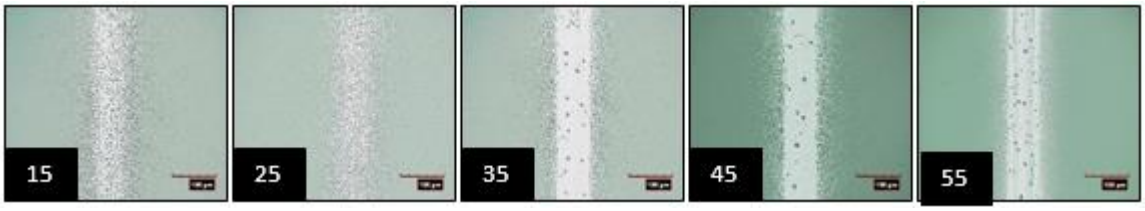

Figure 2.7. Images of line width obtained at different flow rate (sccm)

It has been previously stated the height of the deposition head does not influence the line geometry [19]. The established system in this study does not include sheath gas as in [19] that assists in focusing and preventing over spray which further explains the observations figure 2.7. In the same case, difference in the deposition is to be expected with changing working distance. All the experiments performed in the above study are performed at a constant working of 1mm±0.1mm distance. With the current system, it is essential that we consider the influence of working distance on printing for desired output. Figure 2.8 represents the image of the line printed at different working distances. As the images show in figure 2.8, the optimum line width with least over spray was achieved at 1 mm working distance. Overspray as it appears, is a major constraint in determining the exact line width. It also hampers the electrical properties of the material. Overspray being an entirely different topic, has to be studied based on different factors.

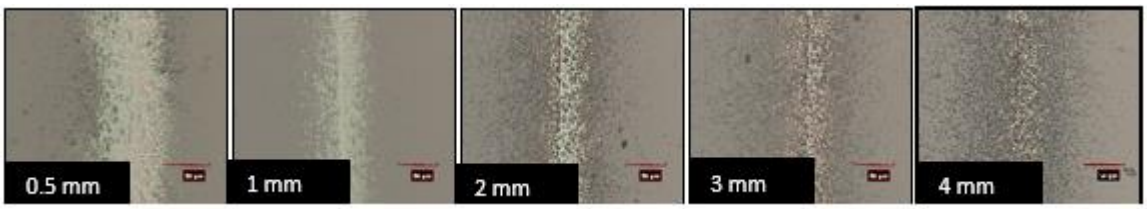

Figure 2.8. Images representing the change in the line width with increasing the deposition height

From the discussion above the following general conclusion can be made for influence of parameters on printing, table 2.1.

Table 2.1. Effect of parameters on printing

Variable	Line Width	Line Thickness
Nozzle Diameter	Increase	Decreases
Carrier Flow Rate	No significant change	Increases
Stage speed	Decreases	Decreases

Along with the above discussed parameters from the aerosol jet printing system, another major factor contributing to the deposition of ink is the nature of substrate. All the plots above show the operation ranges to possible output that the system can give. From figures 2.2 and 2.8, we can vary the combination of parameters to obtain features like individual droplets. It is essential to understand the influence of individual droplets interaction with the surface as any feature

deposited would necessarily comprise of these droplets. This section of study focuses on the deposition of individual droplets and their interaction with the substrate. Efforts were made to understand and interpret the contact angle and nature of the substrates. Contact angle measurements were performed to characterize the nature of surface. The measurements are conducted on a digital-optical contact measurement apparatus, Data Physics-OCA-EC-C1.

A needle of 600 µm diameter was chosen after careful study as discussed above. An average of 20°C was maintained during the process and the stage speed used was 0.5 mm/sec and a low rate 25 sccm was used to deposit droplets with sizes ranging from several microns to sub-microns. The interaction of the silver droplets with surfaces was studied, Titanium Oxide (TiO_2) and Clean glass slide. TiO_2 surface was prepared by spin coating TiO_2 dispersion (US Research Nanomaterials, Anatase, 15% wt.) at 3000 rpm and thermal sintered at 450° C for an hour. Substrate was exposed to the laboratory atmosphere for a day and used for conducting the experiments the following day. This thin film would be referred to as 'TiO_2 surface' in the following discussion.

Aerosol sprayed Ag droplets were deposited on a clean glass slide and glass slide coated with TiO_2. When examined under microscope, glass slide showed size distribution varying from sub microns to a couple of microns, the substrate coated with TiO_2 appears to have a specified range of droplets, an average of 0.5 µm to 1.5 µm in diameter. On the glass slides, it can be noticed that a few of the droplets appeared to wet the surface and a few others seemed spherically standing indicating that the same droplet might have highly dewetted

the surface. The deposition on TiO_2 coated surface has almost no signs of splashes and showed a distinctive spherical geometry. The figure 2.9 represents the particle distribution on glass and TiO_2 surface respectively.

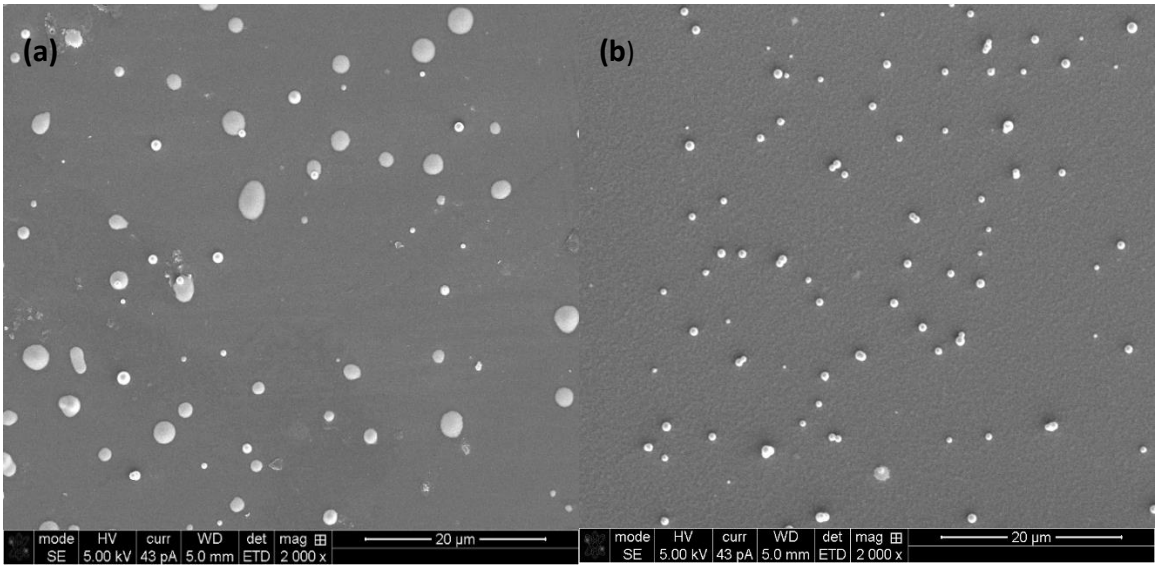

Figure 2.9. SEM images of as-deposited silver droplets on a) Glass slide b) TiO2 coated surface

The histograms shown in figure 2.10 (a, b) represents the particle size distribution on the as- deposited glass slide and on TiO_2 coated surface. The wide range of droplets sizes can be noticed on glass slide in contrast to the size of droplets on TiO_2. It is to be observed that, the on TiO_2 surface, no particle over a size of 1.5 µm was noticed as indicated in the histogram mentioned in the following page. The clear variation in the size distribution encourages further study into the aerosol deposition and its interaction with the substrate.

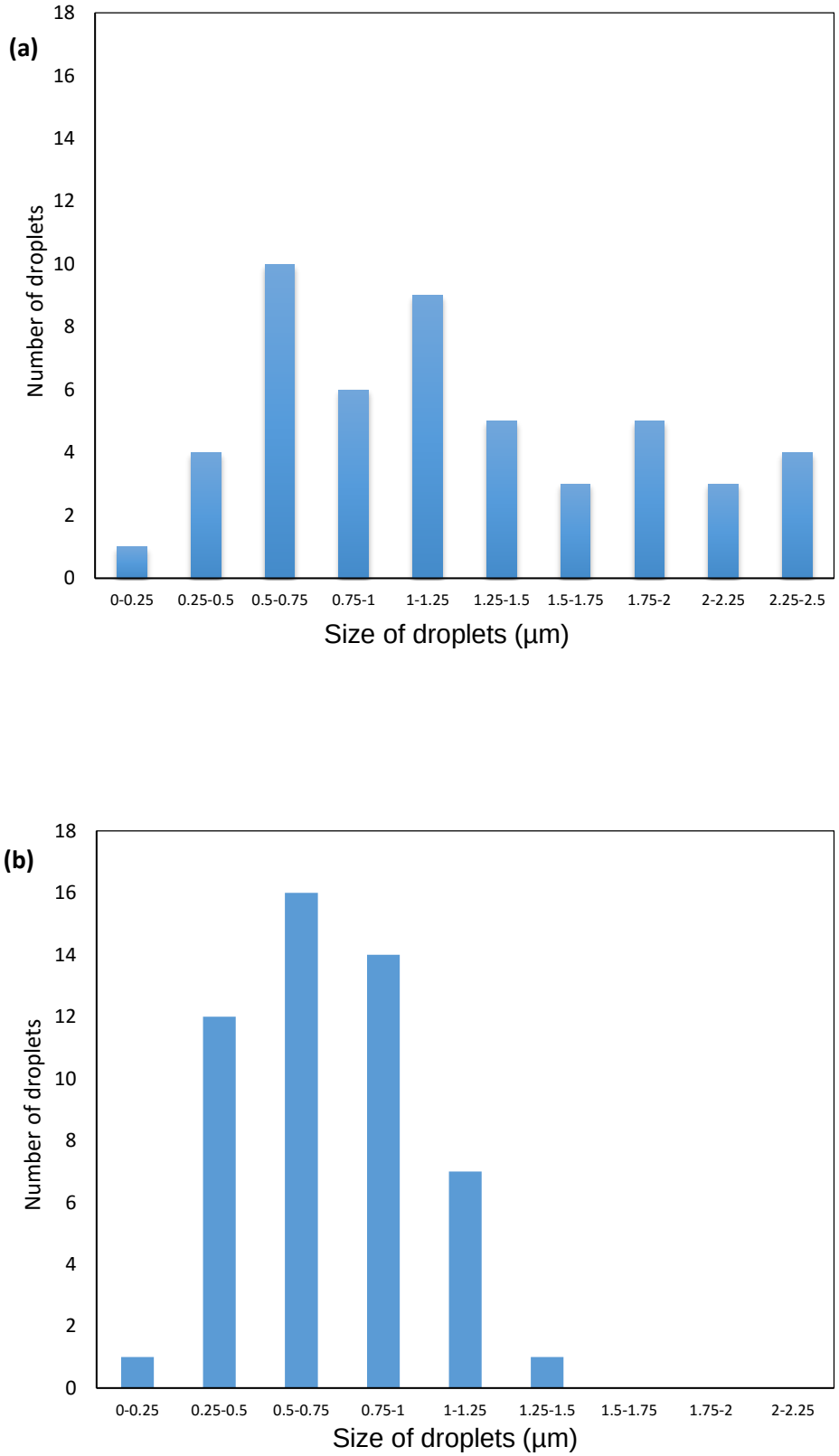

Figure 2.10. Histogram showing the distribution of droplets on (a) TiO_2 coated surface (b) Glass surface

Difference in morphology of the silver droplets deposited on the respective substrates is observed at high magnification in SEM image, figure 2.11.

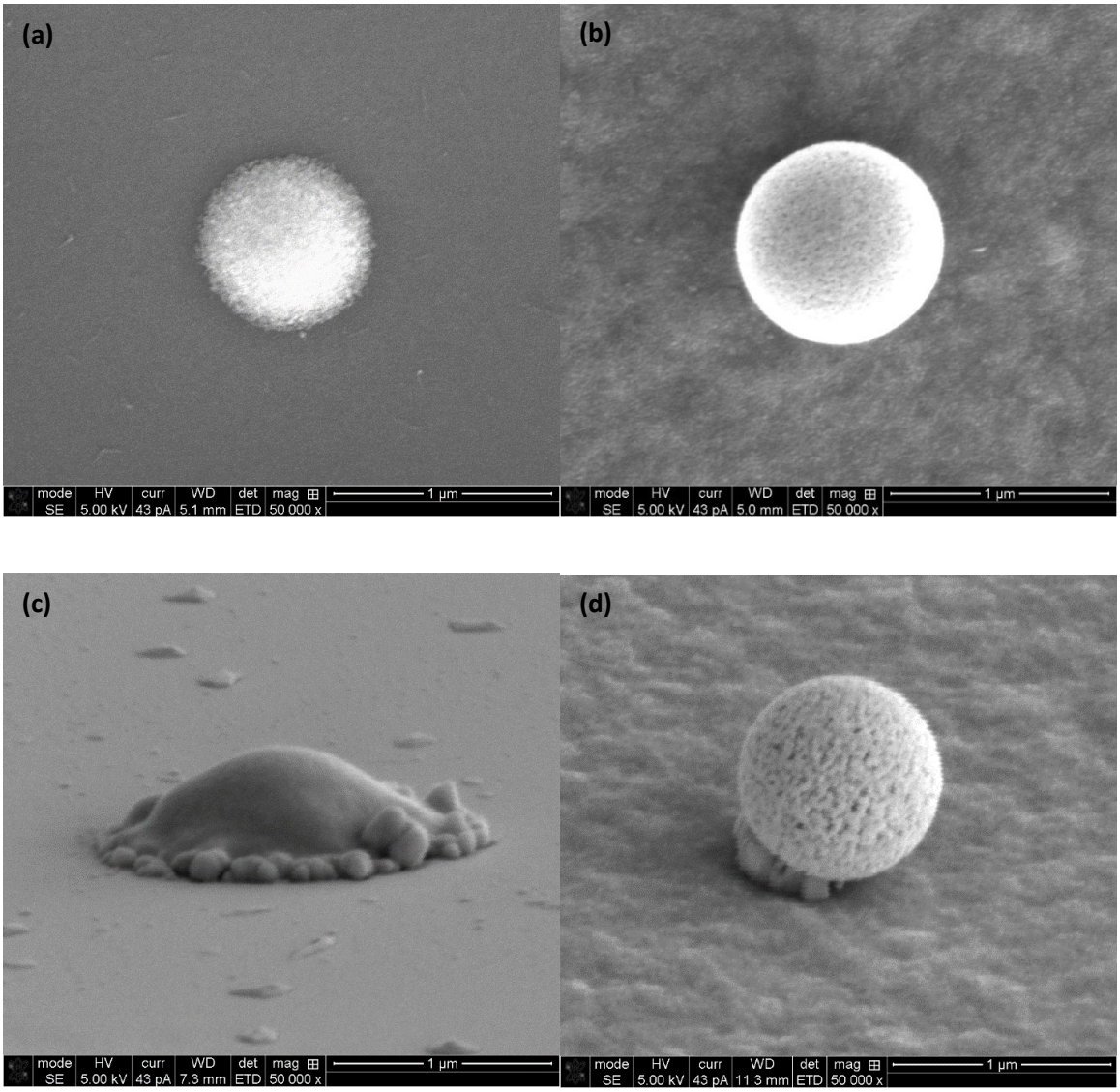

Figure 2.11. High magnification SEM images of as deposited silver droplets.(a, b) Top down view of the deposition on glass slide and TiO_2 coated surface respectively; (c, d) Cross- sectional view of glass and TiO_2 coated surface respectively

The variation in the geometry of the droplet could be observed in the cross sectional view, where obvious de-wetting of the droplets on the TiO_2 coated sample can be observed. To understand the deposition phenomenon, further experiments were to be performed and contact angle measurements to understand the effect of ink on the substrate.

It was proposed that chemical nature of TiO_2 coated surface is different from glass and is highly dependent on the methods adopted to obtain the surface. Metals, Metal alloys [21], metal oxides or any high energy surfaces initially being hydrophilic and oleophilic, turn hydrophobic as a result of progressive organic adsorption [22]. The higher rate of contamination on TiO_2 correlates to the higher surface energy in comparison with a glass surface. This difference in nature of the surface is considered to be one of the contributing factors to the observation in figure 2.11.

Further experiments were performed to understand the effect of solvent on deposition. The droplet sizes were obtained with varying the height of deposition head and by varying the distance between the nebulizer and deposition head. Histogram for the particles deposited at 1 mm deposition head at various tube lengths and presented as follows in figure 2.12. The reduction in the length of the tubes results in the droplets of various sizes.Comparing to the trend in the earlier histogram from figure 2.10 where no droplets larger to 1.5 μm were noticed when depositing over a working distance of 4mm, the histogram in figure 2.12 (d) shows droplets larger in size for the same tubing length.

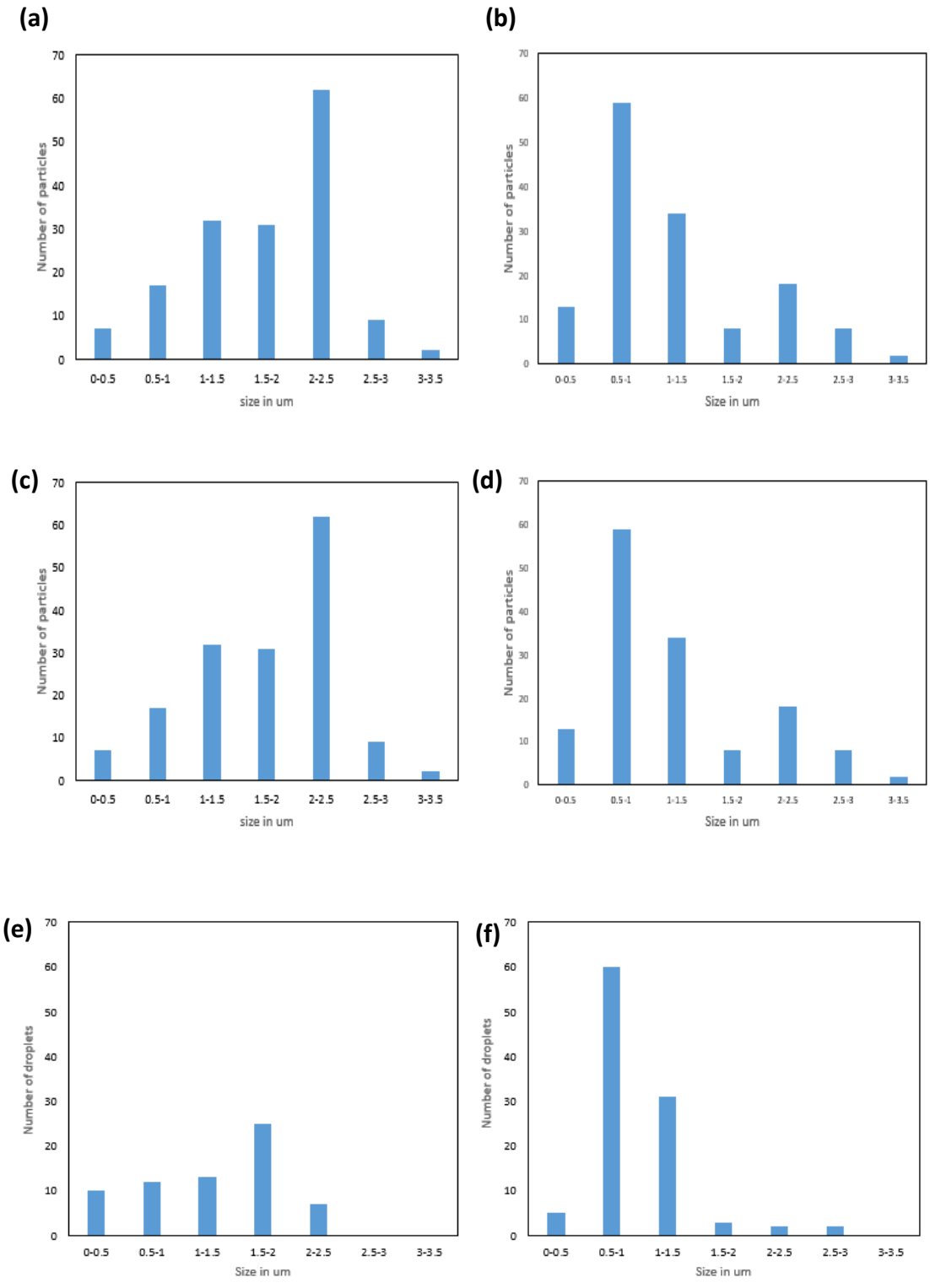

Figure 2.12. Distribution of droplets of various sizes- a) 15” tubing-glass, b) 15” tubing TiO_2, c) 19” tubing-glass, d) 19” tubing- TiO_2 e) 30” tubing-glass f) 30” tubing-TiO_2

Although, the peak of the histograms still remains the same, the reduction in the working distance and change in the tubing length introduces larger droplets that flatten on the surface of TiO_2 due to more solvent. From the distribution, on both the substrates, it becomes evident that when distance to be travelled is increased to 30" tubing, the large droplets that appeared in the other tubes reduce considerably. The total population of the droplets deposited on the substrate seem to reduce at the longer tubing which could be the result of a few droplets settling on the walls of the tubing, suggesting the solvent evaporation.

To validate the influence of the solvent concentration on the spreading of the ink on the substrate, contact angle measurements were performed and rate of spreading was recorded for various concentrations of ink as shown in figure 2.13.

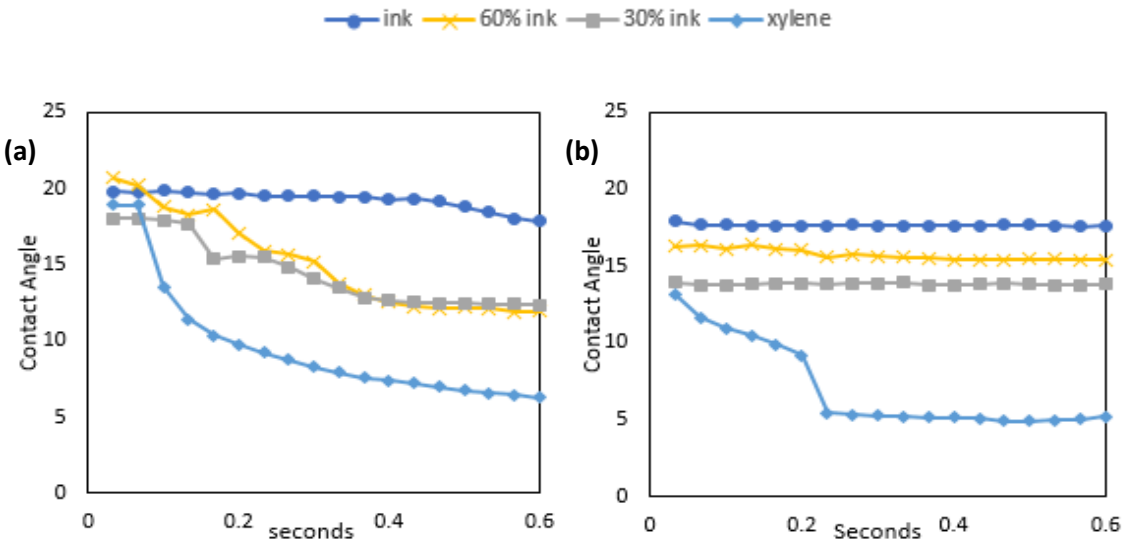

Figure 2.13. Rate of spreading on the surface with change in concentration a) Glass b) TiO_2

Ink concentration when gradually reduced, wets the TiO_2 coated substrate and the rate of spreading on the glass also increases. The commercial ink is mixed with xylene and diluted to 60% ink and 30% ink of the original concentration. Figure 2.13 explains the behavior of 1 µl deposited droplet on the substrates with decreasing concentration. It could be observed that rate of spreading of xylene on TiO_2 coated surface is more than that of the glass. It suggests that, spherical structured droplets formed on the TiO_2 surface might be the result of the Ag particle interaction with the surface as the reduction in the concentration increases the rate of spreading. The above studies justify that nature of the substrate influences the deposition.

2.4 CONCLUSION

As seen from the plots, a 35 sccm with a velocity of 1mm/s results in an average line width of 40 µm. Importance of working distance was uncovered during the experiments and optimized to 1 mm to achieve fine line width and with lesser over spray. The study provided an understanding of the various parameters and provided an operability window to obtain narrow focused lines. Along with the lines and their characteristics, more fundamental approach was made by the introducing the study of individual aerosol deposited droplets. Free standing spherical ink droplets on the TiO_2 coated surface were explained by studying the influence of solvent. Influence of the substrate was realized as a part of this study. This study inspires more research into the influence of substrates on aerosol ink deposition that would result in better printing.

BIBLOGRAPHY

1. A. D. Halvorsen, P. Vaidya, M. Robinson, and D. L. Schulz, “Transforming a laser micromachiner into a direct-write tool for electronic materials,” Journal of MicroElectronics and Electronic Packaging, vol. 5, pp. 116–121, 2008.

2. K. K. B. Hon, L. Li, and I. M. Hutchings, "Direct writing technology-Advances and developments," *Cirp Annals-Manufacturing Technology,* vol. 57, pp. 601-620, 2008.

3. E. Tekin, P. J. Smith, U. S. Schubert, Soft Matter 2008, 4, 703.

4. D. Pesach, A. Marmur, Langmuir 1987, 3, 519.

5. A. Lim, W. H. Lee, H. S. Lee, J. H. Lee, Y. D. Park, K. Cho, Adv. Funct. Mater. 2008, 18, 229.

6. M. J. Renn, “Direct Write System,” USA Patent 7108894 B2,2006.

7. H. D. Rui Liu, Jian Lin, Fangping Shen, Zheng ui and Ting Zhang, "Fabrication of platinum decorated single walled carbon nanotube based hydrogen sensors by Aerosol Jet Printing," 2012.

8. B. King and M. Renn, “Aerosol Jet direct write printing for mil-aero electronic applications,” http://www.optomec.com/ 2009.

9. M. Maiwald, C. Werner, V. Zoellmer, and M. Busse, “INKtelligent printed strain gauges,” Sensors and Actuators, A, vol. 162, no. 2, pp. 198–201, 2010.

10. C. E. Folgar, C. Suchicital, and S. Priya, “Solution-based aerosol deposition process for synthesis of multilayer structures,” *Materials Letters*, vol. 65, no. 9, pp. 1302–1307, 2011.

11. V. R. Marinov, Y. A. Atanasov, A. Khan et al., “Direct-write vapor sensors on FR4 plastic substrates,” IEEE Sensors Journal,vol. 7, no. 6, pp. 937–944, 2007.

12. M. Ha, Y. Xia, A. A. Green et al., “Printed, sub-3V digital circuits on plastic from aqueous carbon nanotube inks,” ACS Nano, vol. 4, no. 8, pp. 4388–4395, 2010.

13. J. H. Cho, J. Lee, Y. Xia et al., “Printable ion-gel gate dielectrics for low-voltage polymer thin-film transistors on plastic,” Nature Materials, vol. 7, no. 11, pp. 900–906, 2008.

14. J. Hoey, D. Thompson, M. Robinson et al., “CAB-DW for 5 μm trace-width deposition of solar cell metallization topcontacts,” in Proceedings of the 34th IEEE Photovoltaic Specialists Conference (PVSC ’09), Philadelphia, Pa, USA, June 2009.

15. M. F. A. M. van Hest, “Direct write approaches for metallization,” in Proceedings of the 2nd Workshop on Metallization of Crystalline Silicon Solar Cells, Cibstabcem, Germany, 2010.

16. Justin M. Hoey, Artur Lutfurakhmanov, Douglas L. Schulz, and Iskander S. Akhatov, ‘A Review on Aerosol-Based Direct-Write and Its Applications for Microelectronics’ , Journal of Nanotechnology, Volume 2012, Article ID 324380.

17. Goth, C.; Putzo, S.; Franke, J. IEEE 61st Electronic Components and Technology Conference (ECTC); Lake Buena Vista, FL, May 31−June 3, 2011 ; IEEE: Piscataway, NJ, 2011; pp 1211−1216.

18. Verheecke, W.; Van Dyck, M.; Vogeler, F.; Voet, A.; Valkenaers,H. 8th International DAAAM Baltic Conference “Industrial Engineering”;Tallinn, Estonia, April 19−21, 2012 ; Danube Adria Association for Automation & Manufacturing: Vienna, Austria, 2012; pp 373-379.

19. Ankit Mahajan, C. Daniel Frisbie and Lorraine F. Francis, “Optimization of Aerosol Jet Printing for High Resolution, High Aspect Ration Silver Lines”, ACS Appl. Mater. Interface 2013, 5, 4856-4864.

20. I.S. Akhatova, J.M. Hoeya, O.F. Swensonb, D.L. Schulza, “ Aerosol focusing in micro-capillaries: Theory and Experiment, Journal of Aerosol Science,39, 2008, 691-709.

21. White, M. L. Goldfinger, G., Ed.; Marcel Dekker,In Clean Surfaces: Their Preparation and Characterization for Interfacial Studies; New York, 1970; p 361.

22. Takeda, S.; Fukawa, M.; Hayashi, Y.; Matsumoto, K. Thin Solid Films 1999, 339, 220.

VITA

Mahati Guntupalli was born in Andhra Pradesh, India on January 7th, 1992. In May 2013, she received her Bachelor of Technology, (B.Tech) in Mechanical Engineering from Guru Nanak Institution, Jawahar Lal Nehru Technological University, Andhra Pradesh, India. She has been pursuing her graduate studies in the Department of Mechanical and Aerospace Engineering at Missouri Science and Technology (Formerly University of Missouri – Rolla) since August 2013. During her stay at Missouri S&T, she held the positions of Graduate Research Assistant and Graduate Teaching Assistant. She received her Master of Science Degree in Mechanical Engineering from Missouri University of Science and Technology, Rolla, USA, May 2016.